

1 **A Physical Impact of Organic Fouling Layers on**
2 **Bacterial Adhesion During Nanofiltration**

3
4
5
6 R. Heffernan¹, O. Habimana¹, A.J.C. Semião², H. Cao¹, A. Safari¹ and E. Casey^{1*}

7
8
9
10
11 ¹*School of Chemical and Bioprocess Engineering, University College Dublin, Co. Dublin, Ireland*

12 ²*School of Engineering, The University of Edinburgh, Edinburgh, United Kingdom*

13 *eoin.casey@ucd.ie

14
15
16
17 *Corresponding author. Mailing address: University College Dublin, School of Chemical and
18 Bioprocess Engineering, Belfield, Dublin 4, IRELAND. Phone: +353 1 716 1877, Email:

19 eoin.casey@ucd.ie

22 **Abstract**

23 Organic conditioning films have been shown to alter properties of surfaces, such as
24 hydrophobicity and surface free energy. Furthermore, initial bacterial adhesion has been
25 shown to depend on the conditioning film surface properties as opposed to the properties of
26 the virgin surface. For the particular case of nanofiltration membranes under permeate flux
27 conditions, however, the conditioning film thickens to form a thin fouling layer. This study
28 hence sought to determine if a thin fouling layer deposited on a nanofiltration membrane
29 under permeate flux conditions governed bacterial adhesion in the same manner as a
30 conditioning film on a surface.

31 Thin fouling layers (less than 50 μm thick) of humic acid or alginic acid were formed on
32 Dow Filmtec NF90 membranes and analysed using Atomic Force Microscopy (AFM),
33 Confocal Microscopy and surface energy techniques. Fluorescent microscopy was then used
34 to quantify adhesion of *Pseudomonas fluorescens* bacterial cells onto virgin or fouled
35 membranes under filtration conditions.

36 It was found that instead of adhering on or into the organic fouling layer, the bacterial cells
37 penetrated the thin fouling layer and adhered directly to the membrane surface underneath.
38 Contrary to what surface energy measurements of the fouling layer would indicate, bacteria
39 adhered to a greater extent onto clean membranes (24 ± 3 % surface coverage) than onto
40 those fouled with humic acid (9.8 ± 4 %) or alginic acid (7.5 ± 4 %). These results were
41 confirmed by AFM measurements which indicated that a considerable amount of energy (10^{-7}
42 $\text{J}/\mu\text{m}$) was dissipated when attempting to penetrate the fouling layers compared to adhering
43 onto clean NF90 membranes (10^{-15} $\text{J}/\mu\text{m}$). The added resistance of this fouling layer was
44 thusly seen to reduce the number of bacterial cells which could reach the membrane surface
45 under permeate conditions.

46 This research has highlighted an important difference between fouling layers for the
47 particular case of nanofiltration membranes under permeate flux conditions and surface
48 conditioning films which should be considered when conducting adhesion experiments under
49 filtration conditions. It has also shown AFM to be an integral tool for such experiments.

50 *Key words: Fouling layer, natural organic matter, atomic force microscopy, nanofiltration,*
51 *bacterial adhesion*

52 1. **Introduction**

53 Since the first large-scale application at the Méry-sur-Oise water filtration plant in France
54 (Cyna et al. 2002), nanofiltration (NF) has become a proven method of water purification. It
55 provides an efficient method of cleaning water of metals, organic matter, organic trace
56 contaminants and divalent salts. However, as these are retained by the NF membrane they
57 build up on the membrane's surface forming a fouling layer which reduces membrane
58 performance (Yuan and Kilduff 2010). Fouling remains the biggest obstacle for the NF
59 industry today.

60 Bacteria present in the water and retained by the NF membrane threaten the most damaging
61 form of fouling: biofouling. As bacteria adhere to the membrane's surface they bind together,
62 excreting exopolymeric substances (EPS) forming a communal film: biofilm (Flemming
63 1997). Bacteria within the biofilm grow and proliferate, expanding the biofilm's influence
64 and further reducing the membrane's filtration capacity (Vrouwenvelder et al. 2008). Bacteria
65 dissociating from mature biofilms pose a threat to further membrane modules or other
66 processes downstream.

67 Efforts to combat this biofouling phenomenon have focused on three approaches: removal,
68 nutrient removal and prevention. The first seeks a method by which existing biofilms can be
69 detached or eliminated, restoring the performance of biofouled membranes using surfactants,
70 chelating agents, chaotropic agents, chlorinated compounds or enzymes (Chen and Stewart
71 2000, Liikanen et al. 2002). The second limits the amount of nutrients, such as carbon or
72 phosphorous, available in water, restricting bacterial growth (Hijnen et al. 2009,
73 Vrouwenvelder et al. 2010) . The third searches for a method by which bacterial adhesion
74 onto virgin membranes can be mitigated. By using surface coatings or functional groups to
75 alter the surface properties of membranes (Ba et al. 2010, Liu et al. 2010) it is thought that

76 the initial bacterial adhesion can be prevented, reducing the risk of biofilm development on
77 the membrane's surface (Rana and Matsuura 2010). Mitigation of bacteria adhesion,
78 however, requires a fundamental understanding of the complex mechanisms governing
79 bacterial adhesion.

80 One of the complications to this preventative approach is the role of conditioning films on the
81 membrane surface during bacterial adhesion. Despite pre-cleaning via coagulation and
82 microfiltration, feed streams from fresh water sources will contain 1-3 mgC/L natural organic
83 matter (Cyna et al. 2002, Ventresque et al. 2000). Within the first few seconds of exposure to
84 the feed stream, a film of these organics a few molecules thick (Lorite et al. 2011) adsorbs on
85 the membrane's surface which can have a significant impact on the surface's properties.
86 Schneider showed the acid-base surface free energy components of conditioned hydrophilic
87 and hydrophobic surfaces to be drastically different to the respective clean substrata
88 (Schneider 1996). Conditioning films were also seen to have a strong influence on solid-
89 liquid and solid-particle interfacial tensions as well as on the surface's free energy of particle
90 adhesion.

91 A few studies have attempted to determine the influence of conditioning films on bacterial
92 adhesion. Although the majority of these studies apply the Derjaguin-Landau-Verwey-
93 Overbeek (DLVO) theory for predicting bacterial adhesion onto conditioned membranes,
94 conflicting results have been reported from these investigations: in one set of studies, organic
95 conditioning films were shown to increase the rate of bacterial adhesion (de Kerchove and
96 Elimelech 2007, Hwang et al. 2012, Hwang et al. 2013), while other studies show the
97 opposite for similar conditioning films (Garrido et al. 2014, Subramani et al. 2009). These
98 opposing reports are due to the complexity of bacterial adhesion and the numerous
99 differences between the experimental approaches taken. Feed composition, bacteria species,
100 adhesion protocols (static or dynamic adhesion), cross-flow and permeation hydrodynamics,

101 as well as sample surface properties are all highly influential on bacterial adhesion and
102 variable between studies (Habimana et al. 2014).

103

104 The inclusion of permeation hydrodynamics in some of the aforementioned studies might
105 explain the observed large discrepancies in bacteria-membrane interactions. As additional
106 molecules of the foulant deposit on the membrane surface (Tang et al. 2007), the film
107 thickness will steadily grow over time resulting in the development of a thin fouling layer 10-
108 50 μm thick as opposed to a conditioning film of a few molecules of thickness. The question
109 then arises as to whether a thin fouling layer governs initial bacterial adhesion under
110 permeation conditions in the same way as a conditioning film created by the initial adsorption
111 of organic matter molecules does?

112

113 The objective of this study was to determine if thin organic fouling layers (less than 50 μm in
114 thickness) govern initial bacterial adhesion in the same way as organic conditioning films (a
115 few molecules thick) have been shown to, in an effort to explain previous conflicting results
116 in the literature involving membrane conditioning during permeation. To achieve this, very
117 thin fouling layers of humic acid (HA) and alginic acid (AA), two of the most predominant
118 natural organic matter (NOM) foulants in fresh water filtration processes (Wilkinson et al.
119 1999), were created and the rate of initial adhesion of *Pseudomonas fluorescens* (a common
120 bacteria species, abundant in soil) onto clean and HA- or AA- fouled NF membranes was
121 quantified.

122

123

124 2. Materials & Methods

125 2.1. Pure Water

126 Laboratory water of the highest quality is imperative when conducting monoculture bacterial
127 studies with membranes (Semiao et al. 2013). The water used throughout this project was
128 Grade 1 pure water ($18.2 \text{ M}\Omega\cdot\text{cm}^{-1}$) obtained from an Elga Process Water System (Biopure
129 15 and Purelab flex 2, Veolia, Ireland), hereafter referred to as MilliQ water.

130

131 2.2. Model Foulants

132 Humic acid (HA; purchased as sodium salt, Sigma-Aldrich, Ireland) and Alginic Acid (AA;
133 purchased as sodium salt, Sigma-Aldrich, Ireland) were used to represent typical fresh water
134 organic foulants. HA was purified of ash content and smaller molecules by performing a
135 series of precipitation-centrifugation steps followed by a week of dialysis and freeze-dried as
136 described by Elimelech et al. (Hong and Elimelech 1997). It was not necessary to further
137 purify AA.

138

139 Fouling solutions were made by dissolving HA (1 mgC/L) or AA (2 mgC/L) in 5 L of MilliQ
140 water. To these solutions 20 mM sodium chloride (NaCl; Sigma-Aldrich, Ireland), 1 mM
141 sodium bicarbonate (NaHCO_3 ; Sigma-Aldrich, Ireland) and 0.5 mM calcium chloride
142 ($\text{CaCl}_2\cdot\text{H}_2\text{O}$; Merck, Ireland) were added to mimic freshwater. The organic foulants were
143 fully dissolved prior to salt addition to avoid calcium complex formation. The salt control
144 used in this study was prepared with the same salt concentrations in MilliQ water without
145 organics.

146

147 For confocal microscopy studies, 1 mg of DAPI (2-(4-amidinophenyl)-1H-indole-6-
148 carboxamide; Sigma-Aldrich, Ireland) was added as a fluorescent staining agent to the 5 L

149 of AA solution (final concentration 0.2 µg/ml). This solution was kept protected from the
150 light throughout preparation and experimentation. No staining agent was required for the
151 naturally fluorescent HA solution.

152

153 2.3. Filtration Membrane

154 The membranes used in this study were flat sheet TFC polyamide NF90 membranes (Dow
155 Filmtec, USA) received as a single flat sheet roll. At equilibrium, membrane samples had a
156 permeate flux rate of $8.7 \pm 0.6 \text{ L m}^{-2} \text{ hr}^{-1} \text{ bar}^{-1}$ and retained $91 \pm 1.5 \%$ of CaCl_2 and NaCl
157 salts in the feed solution at 8 bar and 20°C.

158

159 Prior to experimentation, 27 cm x 5 cm rectangular samples were cut from the flat-sheet roll
160 and soaked in MilliQ water overnight at 4°C to remove their preservative layer. They were
161 subsequently soaked in 30% vol/vol Emsure® absolute ethanol (Merck, Ireland) in MilliQ
162 water for 1.5 hours to disinfect them (Heffernan et al. 2013). The membranes were finally
163 rinsed thoroughly to remove all traces of ethanol.

164

165 2.4. Model Bacterial Strain and Cell Preparation

166 Fluorescent mCherry-expressing *Pseudomonas fluorescens* PCL1701 (Lagendijk et al. 2010)
167 was selected as the model strain in this study. *Pseudomonas* cultures were stored at -80°C in
168 King B broth (King et al. 1954) supplemented with 20% glycerol. Cultured *Pseudomonas*
169 *fluorescens* were obtained by inoculating 100 mL King B broth supplemented with
170 gentamicin at a final concentration of 10 µg/mL using single colonies previously grown on
171 King B agar (Sigma-Aldrich, Ireland) at 28°C. Subsequently, cultures were incubated
172 overnight at 30°C with shaking at 100 rpm and left to grow to late exponential growth stages,
173 corresponding to an Optical Density (OD_{600}) of 1.0.

174

175 For the study of bacterial adhesion onto NOM-fouled NF90 membranes, *Pseudomonas* cell
176 suspensions were standardized by diluting overnight cultures to a final OD_{600} of 0.2 in 200
177 mL of a 0.1 M NaCl (Sigma-Aldrich, Ireland) solution. This ensured a standardized inoculum
178 of approximately 10^8 cells/mL. Cells were then harvested by centrifugation at 5000 rpm for
179 10 min using a Sorval RC5C Plus centrifuge (Unitech, Ireland) and a Fiberlite™ f10-6x500y
180 fixed angle rotor (Thermo Fisher Scientific Inc., Dublin, Ireland). The supernatant was
181 carefully discarded and the pellet re-suspended in a portion of the feed solution using a vortex
182 shaker (Stuart®, Mason technology, Dublin, Ireland).

183

184 2.5. Filtration Setup

185 Filtration experiments were performed using a cross-flow system (Figure 1) comprising of
186 three Membrane Fouling Simulators (MFSs) (Vrouwenvelder et al. 2008) operated in parallel
187 with an active filtration area of 0.008 m^2 each. The system operated in full recirculation mode
188 using a high pressure pump (model P200, Hydra-Cell, UK). Two autoclavable feed tanks
189 (Nalgene, VWR Ireland) were incorporated in the system, with one active at any time and
190 valves in place to allow for switching between tanks without disturbing the flow or system
191 pressure.

192

193 The pressure on the permeate side of the membranes was maintained at atmospheric pressure
194 while the pressure on the feed side was controlled with a back-pressure regulator
195 (KPB1L0A415P20000, Swagelok, UK) and monitored with two pressure transducers (PTX
196 7500, Druck, Radionics, Ireland) on the feed and retentate lines. The feed flow rate was
197 measured using a flowmeter (OG2, Nixon flowmeters, UK) and maintained at 0.66 L/min
198 through each MFS yielding a cross-flow rate of 0.39 m/s. The temperature of the active feed

199 tank was kept constant ($20 \pm 1^\circ\text{C}$) using a Julabo FP50 temperature control bath and a cooling
200 coil. Temperature, flow rate and pressure measurements were recorded with a data-logger
201 (Picolog 1000, PicoTechnology, Radionics, Ireland). Permeate flux measurements of each
202 membrane were calculated by measuring the mass of liquid permeating each membrane in
203 one minute. Permeate samples were obtained via the sample ports and feed samples were
204 taken directly from the feed tank. Samples were not returned to the system after
205 measurement.

206

207 2.6. Filtration System Cleaning Protocol

208 Prior to all filtration experiments the system was thoroughly cleaned. Feed tanks were
209 routinely autoclaved at 120°C , scrubbed with bleach and rinsed repeatedly with MilliQ water
210 to remove any adhered residual cells within the tanks' internal walls. The system was cleaned
211 without a membrane by circulating lab grade IMS (Lennox Laboratory Supplies, Ireland) for
212 one hour, and 0.1 M NaOH for two hours to remove bacteria and traces of the model foulants.
213 The system was rinsed with MilliQ water after each phase of the cleaning regime. The pH of
214 the system was adjusted to 7 by dropwise addition of 5 M HCL or 1 M NaOH over a two
215 hour period, and then finally rinsed with MilliQ water. An additional one hour circulation of
216 20 mM EDTA (VWR, Ireland) was performed prior to IMS circulation in experiments
217 subsequent to those using AA to remove traces of TEPs within the system.

218

219 2.7. Membrane Fouling

220 MilliQ water was filtered overnight with a transmembrane pressure of 15 bar to compact the
221 NF90 membranes and obtain a steady pure-water flux. The feed was then switched via valves
222 to a tank containing the selected fouling solution or salt control solution, without disrupting
223 the flow. The system pressure was adjusted to 8 ± 0.5 bar for each solution to give a permeate

224 flux of $42 \text{ L}\cdot\text{m}^{-2}\cdot\text{hr}^{-1}$ (LMH) from each of the three MFSs. Filtration occurred for 3 hours with
225 the three MFSs in parallel, during which minimal change to the pressure was required to keep
226 the permeate flux constant for each fouling solution despite the development of fouling
227 layers. Samples were taken hourly to monitor and maintain a constant feed conductivity (2.6
228 $\pm 0.05 \text{ mS/cm}$) and pH (8.5 ± 0.5), and to analyse membrane salt retention in the feed and
229 permeate.

230

231 Once the fouling step was finished, one of the fouled MFS devices was removed from the
232 cross-flow system in order to carry out fouling layer characterisation as described in the next
233 sections. The other two MFS devices were left in the cross-flow system in order to carry out
234 the bacterial adhesion experiments. The removed MFS was opened whilst submerged in
235 MilliQ water to preserve the integrity of the fouling layer, and the fouled membrane was
236 removed. For confocal studies three samples were cut from specific locations (inlet, mid-
237 section and outlet) and placed in individual wells of a Lab-Tek® Chamber Slide™ 4-well
238 system (Nunc®; ThermoScientific, Dublin, Ireland) previously filled with MilliQ water.
239 Further samples were taken for fouling layer characterisation via Contact Angle and Zeta
240 Potential. These samples were laid in petri dishes and left to dry in ambient conditions
241 (covered to avoid air particle deposition). A sample for AFM was also taken and submerged
242 in a petri dish of MilliQ water.

243

244 2.8. Adhesion Experiment and Quantification

245 After the removal of one MFS from the cross-flow system, as described above, the feed flow
246 rate was adjusted to maintain a cross-flow velocity of 0.66 L/min ($\text{Re} = 548$) in each MFS in
247 order to keep the same hydrodynamic conditions as the ones used during the fouling step. A
248 bacterial inoculum containing approximately 10^8 cells/mL was added to the fouling solution

249 in the feed tank and recirculated in the system for 30 minutes at the same constant filtration
250 conditions as the ones used during fouling. Permeate flux and conductivity measurements for
251 each membrane cell and a measurement of the feed's conductivity were taken every ten
252 minutes. Every experiment (i.e. fouling step + fouling characterisation + bacterial adhesion)
253 was repeated at least twice to ensure reproducibility.

254

255 The two MFS cells were separated from the system at the end of the bacterial adhesion
256 experiments, and carefully opened whilst submerged in MilliQ water in order to preserve the
257 integrity of the fouling layer. The fouled membranes were removed, three pieces cut from
258 different locations (inlet, mid-section and outlet) of the membrane and each sample was
259 placed at the bottom of small petri dishes submerged in MilliQ water. Bacterial cells adhered
260 to the fouled membranes were then observed under an epi-fluorescence microscope
261 (Olympus BX51) using a 10X objective. Fluorescent mCherry-tagged *Pseudomonas* cells
262 were detected using the microscope's U-MNG or U-MWIB excitation/emission filter cubes
263 systems. Ten micrographs were obtained at random points from each membrane sample. Cell
264 surface coverage (%) was then determined, from grayscaled and thresholded acquired images
265 for each membrane using ImageJ® software, a Java-based image processing program
266 (<http://rsbweb.nih.gov/ij/>). At the concentration used, the HA layer's natural fluorescence did
267 not interfere with mCherry fluorescence signals.

268

269 2.9. Structural Analysis of Fouled Membranes

270 To assess the organic fouling layers on the membranes, horizontal-plane images of fouled
271 membrane samples in their Lab-Tec® wells were acquired using an Olympus Fluoview FV
272 1000 Confocal microscope.

273

274 The excitation wavelength used for detecting DAPI-stained SA was 405 nm, and emitted
 275 fluorescence was recorded within the range of 420 to 460 nm (Lee et al. 2011). For HA
 276 conditioned membranes, an excitation wavelength of 488 nm and auto-fluorescence was
 277 recorded at 500-550 nm. Images (1269 μm x 1269 μm) were collected through a UPLSAPO
 278 10x objective (numerical aperture NA 0.4) with a z-step of 1 μm . 3D projections were
 279 performed with Zen software (Zeiss). The structural quantification of the NOM conditioning
 280 layer (biovolume, surface coverage, thickness and roughness) was performed using the
 281 PHLIP Matlab program developed by J. Xavier
 282 (<http://sourceforge.net/projects/phlip/>)(Mueller et al. 2006).

283

284 2.10. Surface Properties of Fouled Membranes

285 The Lifshitz-van der Waals (γ_{LW}), electron-donor (γ^-) and electron-acceptor (γ^+) surface
 286 tension components of dehydrated treated NF90 membrane samples (S) were determined by
 287 measuring contact angles using the following expression:

$$288 \cos\theta = -1 + 2 \left(\gamma_S^{LW} \gamma_L^{LW} \right)^{\frac{1}{2}} / \gamma_L + 2 \left(\gamma_S^+ \gamma_L^- \right)^{\frac{1}{2}} / \gamma_L + 2 \left(\gamma_S^- \gamma_L^+ \right)^{\frac{1}{2}} / \gamma_L \quad (1)$$

289 Contact angles (θ) and surface energy measurements (γ_S) of dehydrated compacted NF90
 290 membrane were measured at room temperature using a goniometer (OCA 20 from
 291 Dataphysics Instruments) with three static pure liquids (L): deionised water, diiodomethane
 292 and ethylene glycol.

293 The Lewis acid-base component was deduced from:

$$294 \gamma_S^{AB} = 2\sqrt{\gamma_S^+ \gamma_S^-} \quad (2)$$

295 And the total surface energy was defined by:

$$296 \gamma_S = \gamma_S^{AB} + \gamma_S^{LW} \quad (3)$$

297 The interfacial free energy of adhesion (ΔG_{132}) was calculated from these derived
 298 components using the method laid out by Brant and Childress (Brant and Childress 2002).

299 Values for bacterial surface components were taken from a study on *Pseudomonas*
300 *fluorescens* by Smets et al.: $\gamma^- = 34.9 \text{ mJ/m}^2$, $\gamma^+ = 0.22 \text{ mJ/m}^2$, and $\gamma^{\text{LW}} = 30.8 \text{ mJ/m}^2$ (Smets
301 et al. 1999).

302

303 Samples for zeta potential analysis were dried in air overnight, rehydrated in MilliQ water for
304 an hour and then submerged in a 5 mM NaCl solution overnight as described previously by
305 Elimelech (Xie et al. 2013). There was a slight dissolution of the fouling layer upon
306 introduction into the salt solution but it was greatly minimised by the dehydration-rehydration
307 step. Streaming potential measurements of the fouled membranes were conducted using a
308 ZetaCad system (CAD instruments, France) with a 5 mM NaCl (pH 8, 0.5 mS/cm) solution
309 streamed through a 150 μm channel between two similarly fouled samples. By varying the
310 flow rate through the channel and measuring the voltage difference across the chamber the
311 zeta potential was calculated.

312

313 2.11. Atomic Force Microscopy

314 Surface layer stiffness and adhesive properties of fouled and clean membranes were
315 characterised by analysing indentation and retraction curves obtained from AFM-based Force
316 Spectroscopy measurements. Force measurements were performed using a JPK NanoWizard
317 II BioAFM (JPK Instruments, Germany) integrated with an inverted optical microscope
318 (Nikon, Japan) and a Hamamatsu CCD camera. This ensemble was enclosed in an acoustic
319 isolation chamber, and placed on a vibration isolation table (TS-150, JRS Scientific
320 Instruments, Switzerland).

321

322 A commercial silicon nitride cantilever with a sharp triangular silicon nitride tip of 60 nm
323 radius (DNP-10, C type, Bruker, UK) was used in this study. The spring constant of the

324 cantilevers was calibrated as 0.142 N/m at the room temperature, using the thermal noise
325 method. Force curves were measured while approaching within 0.5 μm from the salt control
326 membrane's surface and while approaching and penetrating the top 0.5 - 1 μm of the created
327 AA and HA fouling layers. The area between the two force curves for each sample was
328 calculated computationally. In each case this area was subdivided into two areas by the
329 horizontal line representing 0 N, the area above this line was recorded as the 'energy
330 dissipated in approach' while the area below it was recorded as the 'energy dissipated in
331 retraction'. For comparative reasons these area values were divided by the width of the
332 curves (distance travelled by the tip) to correct the values to a full 1 μm .

333

334 After several force curve measurements, several force curves were recorded on a clean
335 surface (i.e. glass) in order to observe the possible residual forces on the retraction curves due
336 to the tip contamination. When contaminated, the cantilever was carefully rinsed with ethanol
337 and Milli-Q water, before being placed in UV Ozone cleaner (ProCleaner, Bioforce
338 Nanosciences, USA). Force curves were collected at a velocity of 2 $\mu\text{m/s}$ up to a force set-
339 point limit of 18 nN.

340

341 3. Results & Discussion

342 3.1. Surface Characterisation of the Fouling layer

343 Images taken with the confocal microscope were combined to create image stacks from
344 which the density, height and roughness of the created fouling layers were determined at
345 three locations along the length of the flow channel (Figure 2).

346 The AA fouling layers created had an average thickness of $25 \pm 4 \mu\text{m}$ and a surface coverage
347 higher than 70% along the length of the membrane. This layer was very reproducible with
348 less than 20% difference between fouling layers created for most parameters. The largest

349 variations were seen in the roughness measurements which may be associated with AA's
350 tendency to bind with calcium to create clumps (Listiarini et al. 2009).

351

352 The HA fouling layer in contrast shows an increase in thickness in the middle section of the
353 membrane; the fouling layer bulges by 66% from $20 \pm 4 \mu\text{m}$ at the inlet to a maximum of 34
354 $\pm 8 \mu\text{m}$ before returning to a thickness of $25 \pm 7 \mu\text{m}$ at the outlet. This bulge is accompanied
355 with a 20% drop in surface coverage and a steady rise in roughness along the length of the
356 flow channel. It appears that HA deposits as a thin even layer at the inlet of the channel,
357 becoming rougher and less evenly dispersed for the midsection and the outlet. This trend was
358 evident in each of the membrane samples studied. The largest variations between experiments
359 were again in the roughness measurements, especially at the outlet of the MFS.

360

361 The average roughness of each fouling layer was calculated by multiplying the layer
362 thickness by the Fouling Layer Roughness factor presented in Figure 2d (Heydorn et al.
363 2000). The AA layer has an average roughness along the length of the membrane of 5.3 ± 0.7
364 nm while the HA layer increases along the membrane length, from 2.3 nm at the inlet to 9.4
365 nm at the outlet. These values are smoother than the values reported for a clean NF90
366 membrane which has an average roughness of 60 nm (Xu et al. 2006).

367

368 The surface coverage and thickness measurements of the independent experiments show that
369 the fouling layers created under the same fouling conditions are reproducible. The small
370 variances between the layers may be associated with the large range of molecule sizes in each
371 substance or with the heterogeneous nature of the membrane surface which can lead to flux
372 hotspots (Ramon and Hoek 2013). Errors may also have occurred due to slight dissociation of

373 the fouling layer upon exposure to MilliQ water when the samples were transferred from the
 374 MFS to the confocal sample chambers.

375

376 3.2. Surface Energy

377 Within 100 nm of a surface the forces dominating a single bacterial cell's movements will be
 378 the van der Waal's force, the Lewis acid-base interaction and repulsion from the electrostatic
 379 double-layer (Brant and Childress 2002).

380

381 *Table 1: Measured zeta potential (ζ) and contact angle values, and derived electron acceptor (γ^+), electron
 382 donor (γ^-), Lifshitz van der Waals (γ^{LW}), Acid-base (γ^{AB}), total surface tension (γ^{total}) and total interfacial free
 383 energy of adhesion (ΔG_{132}) of the surface energies of NF90 membranes fouled with humic acid, alginic acid or
 384 with a salt control. Contact angle measurements and derived components of surface energy were taken from 20
 385 measurements on two independent samples. The average values and standard errors values are shown.*

	Salt Control	Humic Acid	Alginic Acid
Contact Angle ($^\circ$)	43.6 \pm 2.75	43.5 \pm 0.45	23.6 \pm 0.5
γ^- (mJ/m ²)	43.0 \pm 0.14	39.8 \pm 0.4	38.0 \pm 0.21
γ^+ (mJ/m ²)	0.06 \pm 0.011	0.35 \pm 0.045	0.18 \pm 0.037
γ^{LW} (mJ/m ²)	40.13 \pm 3.48	51.79 \pm 1.03	72.38 \pm 0.95
γ^{AB} (mJ/m ²)	2.88 \pm 0.3	7.22 \pm 0.53	4.77 \pm 0.54
γ^{total} (mJ/m ²)	43.02 \pm 3.42	59.01 \pm 1.48	77.15 \pm 1.41
ΔG_{132} (mJ/m ²)	19.1	14.7	11.38
ζ (mV)	-23.1 \pm 0.71	-25.7 \pm 0.007	-23.1 \pm 1.23

386

387

388 The obtained results (Table 1) show that the addition of the HA fouling layer did not change
 389 the shape of a droplet compared to the droplet shape on the clean membrane. The addition of
 390 an AA layer, however, caused the membrane to become more hydrophilic with a reduction in
 391 contact angle from 43.6 \pm 2.75 $^\circ$ to 23.6 \pm 0.5 $^\circ$. To gain a better understanding of the forces
 392 involved a more expansive analysis was undertaken.

393

394 The derived components of surface energy reveal numerous changes that have occurred upon
395 addition of the fouling layer. The apolar Lifshitz-van der Waals component has increased
396 from $40.13 \pm 3.48 \text{ mJ/m}^2$ of the clean membrane to $51.79 \pm 1.48 \text{ mJ/m}^2$ and 72.38 ± 0.95
397 mJ/m^2 for membranes fouled with HA and AA, respectively. The polar Lewis acid-base
398 component was also higher for the two layers of fouling than for the clean membrane, but to a
399 much lesser extent.

400

401 Calculations of the interfacial free energy of adhesion (ΔG_{132}) yielded lower resultant
402 energies for HA and AA, 14.7 mJ/m^2 and 11.38 mJ/m^2 , respectively, than for the salt control
403 membrane, with 19.1 mJ/m^2 . Lower energies of adhesion indicate less bacterial repulsion and
404 therefore less resistance to adhesion (Subramani and Hoek 2008). This suggests that based on
405 contact angle measurements, bacteria should adhere to the largest extent on the AA fouled
406 membrane, to a lesser extent on the HA fouled membrane and to the lowest extent on the salt
407 control, non-fouled membrane.

408

409 3.3. Zeta Potential

410 The addition of a fouling layer did not appear to significantly affect the zeta potential of the
411 membrane (Table 1), hence not contributing to differences in bacterial adhesion. While the
412 HA layer exhibited a statistically more negative zeta potential, in the context of a study by Li
413 et al. (Li and Logan 2004) who correlated bacterial adhesion to zeta potential over the range 0
414 to - 60 mV, a difference of 2 mV is not expected to be great enough to have any appreciable
415 effect on bacterial adhesion. There is a notable risk of error in these measurements, however.
416 Fresh fouling layers subjected to the salt solution used in the streaming potential analysis
417 tended to dissociate from the membrane. It was therefore necessary to allow the samples to

418 dry and re-soak the samples in MilliQ water prior to measurement, as has been shown in
419 previous studies (Xie et al. 2013). This protocol leads to a compaction and re-expansion of
420 the fouling layer; furthermore, it may also lead to leaching of certain salts from within the
421 layer, which may have altered the zeta potential of the layer.

422

423 As the streaming potential measurements were taken with a liquid of different ionic strength
424 than the fouling solution, the zeta potential values shown should not be used as a direct
425 indication of bacterial adhesion; they are merely for comparative purposes.

426

427 3.4. Atomic Force Microscopy

428 AFM was employed to compare the physical properties of the fouling layers. Repulsive
429 forces were measured when approaching the clean membrane samples and while penetrating
430 into the top of the fouling layers, whilst adhesive forces were measured when retracting the
431 probe from each sample (Figure 3) .

432

433 Approaching the clean membrane's surface required a small amount of energy (10^{-15} J/ μm) as
434 the probe was repelled by the membrane's surface charge. With the addition of the fouling
435 layers, however, the probe required a much larger magnitude of energy (10^{-7} J/ μm) per
436 micron of movement. The probe in this case was still more than 20 μm away from the
437 membrane's surface and thus would not have felt the membrane's repulsion; the energy
438 dissipated is hence related to the resistance to penetration of the relatively dense fouling layer
439 itself.

440

441 When the probe was retracted from the fouling layers there was a notable strain as the sticky
442 fouling layers resisted the probe's removal. The 10^{-8} J/ μm required to escape the HA and AA

443 layers is once again many orders of magnitude higher than the 10^{-16} J/ μm required to retract
444 the probe from the salt control membrane.

445

446 On average the energy required to retract from the membrane or fouling layers was one order
447 of magnitude lower than the energy required to approach or penetrate them. This agrees with
448 the positive values of ΔG_{132} shown previously that suggested the overall charge on the
449 membrane's surface (fouled and not fouled) would most likely repel bacteria. These results
450 show a notable resistance to penetration and escape from a fouled membrane that is not
451 present for the salt control. This suggests that the layers may act as an obstacle resisting
452 bacterial penetration leading to a lower rate of bacterial adhesion onto the NF membrane
453 surface.

454 On average more energy was dissipated when penetrating the HA layer (2.33×10^{-7} J/ μm)
455 than the AA layer (1.32×10^{-7} J/ μm). The reverse was true when retracting the probe which
456 exhibited a higher average dissipation of energy moving through the AA layer (3.3×10^{-8}
457 J/ μm) than the HA layer (1.18×10^{-8} J/ μm). These results would therefore suggest that
458 bacterial adhesion would occur to a greater extent within the AA layer, as it is more likely
459 that bacterial cells would penetrate the layer and less likely that they would be able to escape
460 it. These differences are, however, of a much smaller magnitude than those described
461 previously between fouled and clean NF90 membranes.

462

463 3.5. Bacterial Adhesion onto Fouled Membranes

464 A previous study showed that in the presence of a thin conditioning film of organic
465 compounds on a surface (a few molecules of thickness), bacterial cells deposited on top of the
466 film (Hwang et al. 2013). In contrast, microscopic analysis of bacterial adhesion onto organic
467 fouled NF90 membranes under permeate flux conditions showed this was not the case. All of

468 the bacteria were seen to penetrate the HA and AA fouling layers and adhere directly to the
469 NF90 membrane's surface. No bacteria were seen on top of the organic fouling layer or
470 suspended within it. The surface coverage values shown in Figure 4 are hence representative
471 of the bacteria adhered at the membrane's surface level, within the fouling layer in the case of
472 HA and AA.

473

474 Despite indications from the surface energy measurements that the fouling layers would
475 promote bacterial adhesion, the results of microscopic studies show considerably greater
476 numbers of bacteria adhering to the unfouled salt control membrane (Figure 4). This suggests
477 that the forces measured via AFM are a more accurate indicator of the extent of bacterial
478 adhesion under permeate flux onto thinly organic fouled membranes than those measured via
479 surface energy studies, the most commonly used technique to characterise conditioning film
480 layers and explain bacterial adhesion (Hwang et al. 2013, Subramani et al. 2009).

481

482 Of the two fouling layers, HA is slightly more prone to bacterial adhesion ($t(78) = 4.3$, $p <$
483 0.001 ; $9.8 \pm 4\%$ surface coverage) than the AA layer ($7.5 \pm 4\%$ surface coverage) as can be
484 seen in Figure 4, while contact angle measurements indicated that bacterial adhesion was
485 expected to occur mainly in the AA fouling layer. Despite AFM results also indicating a more
486 prone adhesion to AA fouling layers compared to HA layers, the differences expected were
487 very small (1.32×10^{-7} J/ μm and 2.33×10^{-7} J/ μm , respectively). The difference of bacterial
488 adhesion between the two types of fouling layers tested is however only one sixth of the
489 difference between fouled and clean membranes.

490

491 Rougher membrane surfaces have been shown to have a higher propensity for bacterial
492 adhesion as the heterogeneity of the surface yields rough features which are more favourable

493 sites for surface-bacteria bonding (Subramani and Hoek 2008). There is a positive correlation
494 between cell surface coverage and average surface roughness for clean and fouled NF90
495 membranes in this experiment. However the bacteria did not bond directly to the surface of
496 the fouling layers, hence a correlation between adhesion and surface roughness would be
497 misleading, as will be discussed in the next section.

498

499 Subramani and Hoek discussed the forces acting upon bacteria in their 2008 study with clean
500 NF and RO membranes (Subramani and Hoek 2008). They described six forces which
501 dominate bacteria adhesion in cross-flow configuration. These are: cross-flow lift (F_{CL}),
502 permeate drag (F_{PD}), gravity (F_G), Lifshitz-van der Waal's force (F_{LW}), electrostatic double
503 layer (F_{EL}), and acid base force (F_{AB}). At a distance greater than 100 nm from the
504 membrane's surface the first three of these forces dominate bacterial movement. If the drag
505 due to the permeating liquid is strong enough to counteract the lifting force associated with
506 cross-flow, the bacteria will be drawn towards the membrane surface. Once the bacteria are
507 within 100 nm of the membrane's surface their movement is subjected also to the short range
508 forces such as Lifshitz-van der Waal's forces. If the additional attraction of the Lifshitz-van
509 der Waal's force is enough to overcome the repulsion of the electrostatic double layer and the
510 acid base interactions, the bacteria is likely to attach to the membrane (assuming both
511 membrane and bacteria are negatively charged as is the case for this study).

512

513 Correlations between bacterial adhesion and hydrophobicity, or with other membrane surface
514 energy properties, assume that bacteria have an equal probability of approaching within a
515 distance of 100 nm from the surface of the membrane. This is an acceptable assumption for
516 clean membranes or for studies of conditioning films, which are no more than a few
517 nanometres thick. For fouling layers thicker than 100nm, however, bacteria first interact with

518 the fouling layer outside this 100 nm region. The additional physical force required to
519 penetrate the fouling layer has a greater influence on bacterial transport than the surface
520 energy effects, as shown above where fouling layers of different surface properties but
521 similar thickness were subject to similar amounts of bacterial adhesion. The permeate drag
522 force must now overcome the fouling layer's resistance as well as the cross-flow lift in order
523 for bacteria to reach a proximity to the membrane surface whereby short range surface
524 energy forces can take effect. In this case surface energy effects of the fouling layer of the
525 membrane surface alone cannot be used to analyse bacterial adhesion through fouling
526 layers thicker than 100 nm.

527

528 3.6. Bacterial Adhesion Profile Along the Length of the Membrane

529 Microscopic analysis of the fouled membranes showed a significant change in the number of
530 bacteria adhered onto different sections along the length of the membrane. Despite the
531 heterogeneous nature of NF membranes, the average surface properties on a micron scale
532 should not change along the length of the membrane surface. Similarly, with an average
533 bacteria count of 10^7 cells/mL in the feed tank, the feed solution flowing across the
534 membrane surface should not change significantly in bacterial concentration along the length
535 of the channel. It is therefore unexpected that bacteria would adhere to different extents at the
536 inlet, mid-section and outlet.

537

538 One of the six forces mentioned previously will however change along the channel length. As
539 water permeates the initial sections of the membrane the pressure within the channel slightly
540 drops leading to a lower driving force for permeation and thus lower permeate drag forces in
541 subsequent stages of the channel (Geissler and Werner 1995). This permeate drag gradient

542 could result in a gradient in initial bacterial adhesion, with a high concentration of bacteria at
543 the inlet and a lower adhesion at the outlet.

544

545 Furthermore, Busscher and van der Mei described a pseudo-end phase to initial bacterial
546 deposition whereby adhesion slows down due to inter-bacterial blocking (Busscher and van
547 der Mei 2006) caused by the repulsion effect of bacteria adhered to the membrane. Bacterial
548 cells approaching a densely populated membrane surface are likely to be repelled, adhering
549 instead downstream to a more sparsely populated region. In this way an even lawn of
550 bacterial cells eventually develops across the membrane surface.

551

552 This is seen for the salt control membrane which had an even 24 ± 3 % surface coverage of
553 bacteria on each section of the membrane (Figure 5). This is indicative that within the 30
554 minutes of adhesion the system reached the pseudo-end stage. For the fouled membranes,
555 however, a significant reduction in bacterial adhesion was seen along the membrane channel,
556 indicating that a pseudo-end stage was not reached.

557

558 Adhesion through the HA layer fell from 15.2 ± 2 % bacterial surface coverage at the inlet to
559 7.3 ± 2 % and 7.0 ± 2 % in the mid-section and outlet, respectively. A lesser reduction was
560 seen for adhesion through the AA layer: 11.4 ± 4.5 % (inlet), 6.5 ± 2.4 % (mid-section) and
561 4.5 ± 1.2 % (outlet). These reductions on the latter stages of the fouled membranes do not
562 correlate with any of the trends in membrane properties quantified with the confocal
563 microscope (Figure 2). The reducing trend in adhesion to the HA fouled NF90 membrane
564 directly contrasts with the increasing trend in HA surface roughness (Figure 2 d): roughness
565 is therefore not a dominant factor during bacterial adhesion onto organic fouled NF
566 membranes. The same applies to AA: despite the AA roughness not changing along the

567 membrane length, bacterial adhesion decreases substantially from the inlet ($11.4 \pm 4.5 \%$) to
568 the outlet ($4.5 \pm 1.2 \%$). This bacterial adhesion trend is instead indicative of the permeate
569 drag force gradient along the channel length.

570

571 Bacteria in the initial sections of the membrane are subjected to the strongest permeate drag
572 force and thus are most likely to overcome the penetration resistances of the fouling layers
573 measured by the AFM. In the latter sections of the channel however the lower drag forces
574 result in fewer bacteria penetrating the fouling layers.

575

576 As was the case with the AFM results, the differences in adhesion between the fouling layers
577 for each section are insignificant compared to the differences between fouled and non-fouled
578 membranes. With a maximum surface coverage of 15%, adhesion onto the fouled membranes
579 has not reached the pseudo-end stage seen with the non-fouled membranes ($24 \pm 3\%$ surface
580 coverage along the entire membrane). The uneven distribution of bacteria along the channel
581 length may therefore be due to absence of inter-bacterial blocking across the membrane
582 surface.

583

584 4. **Conclusion**

585 Fouling layers of Humic Acid and Alginic Acid between 20 and 35 μm thick were shown to
586 decrease bacterial adhesion in cross-flow filtration under permeate flux conditions. The
587 opposite trend would be expected based on surface energy results obtained from contact
588 angle measurements of the fouling layer deposited on the membrane surface and assuming
589 the bacteria would adhere on the fouling layer surface. All adhered bacterial cells were
590 instead seen to adhere directly onto the membrane surface in all experiments and were not
591 entrained in the fouling layers. AFM proved to be a useful tool in this study as it showed that

592 bacteria require a much greater magnitude of energy to reach the membrane's surface when
593 penetrating the NOM fouling layers.

594

595 This study has shown that bacterial adhesion in the presence of a fouling layer and permeate
596 flux to be notably different from conditioning film experiments in which bacteria adhere onto
597 an ultrathin conditioning layer. It is imperative that future studies of bacterial adhesion
598 ontoconditioning films or fouling layers under permeate flux conditions are aware of this
599 difference and monitor the created layer's thickness to avoid potential errors arising from
600 layer resistance.

601

602 Further research in this area is required to study the impact of this decreased adhesion on
603 biofouling development in the absence and presence of an organic matter fouling layer and
604 for different environmental conditions such as the presence of absence of nutrients.

605

606 5. **Acknowledgements**

607 This research was supported by the European Research Council (ERC), project 278530,
608 funded under the EU Framework Programme 7 and also with the financial support of Science
609 Foundation Ireland under Grant Number "SFI 11/RFP.1/ENM/3145. The authors would like
610 to thank Mr. Pat O'Halloran for his invaluable technical assistance, and Mr. Liam Morris for
611 the construction of the MFS devices. The authors especially thank Dr. Ellen L. Lagendijk
612 from the Institute of Biology Leiden, Netherlands for the gift of the *Pseudomonas fluorescens*
613 WCS365, PCL1701

614 6. References

- 615 Ba, C., Ladner, D.A. and Economy, J. (2010) Using polyelectrolyte coatings to improve
616 fouling resistance of a positively charged nanofiltration membrane. *Journal of Membrane*
617 *Science* 347(1–2), 250-259.
- 618 Brant, J.A. and Childress, A.E. (2002) Assessing short-range membrane–colloid interactions
619 using surface energetics. *Journal of Membrane Science* 203(1–2), 257-273.
- 620 Busscher, H.J. and van der Mei, H.C. (2006) Microbial adhesion in flow displacement
621 systems. *Clinical microbiology reviews* 19(1), 127-141.
- 622 Chen, X. and Stewart, P.S. (2000) Biofilm removal caused by chemical treatments. *Water*
623 *Research* 34(17), 4229-4233.
- 624 Cyna, B., Chagneau, G., Bablon, G. and Tanghe, N. (2002) Two years of nanofiltration at the
625 Méry-sur-Oise plant, France. *Desalination* 147(1–3), 69-75.
- 626 de Kerchove, A.J. and Elimelech, M. (2007) Impact of alginate conditioning film on
627 deposition kinetics of motile and nonmotile *Pseudomonas aeruginosa* strains. *Applied and*
628 *Environmental Microbiology* 73(16), 5227-5234.
- 629 Flemming, H.-C. (1997) Reverse osmosis membrane biofouling. *Experimental Thermal and*
630 *Fluid Science* 14(4), 382-391.
- 631 Garrido, K.D., Palacios, R.J.S., Lee, C. and Kang, S. (2014) Impact of conditioning film on
632 the initial adhesion of *E. coli* on polysulfone ultrafiltration membrane. *Journal of Industrial*
633 *and Engineering Chemistry* 20(4), 1438-1443.
- 634 Geissler, S. and Werner, U. (1995) Dynamic model of crossflow microfiltration in flat-
635 channel systems under laminar flow conditions. *Filtration & Separation* 32(6), 533-537.
- 636 Habimana, O., Semiao, A.J.C. and Casey, E. (2014) The role of cell-surface interactions in
637 bacterial initial adhesion and consequent biofilm formation on nanofiltrationreverse osmosis
638 membranes. *Journal of Membrane Science* 454, 82-96.
- 639 Heffernan, R., Semião, A.J.C., Desmond, P., Cao, H., Safari, A., Habimana, O. and Casey, E.
640 (2013) Disinfection of a polyamide nanofiltration membrane using ethanol. *Journal of*
641 *Membrane Science* 448(0), 170-179.
- 642 Heydorn, A., Nielsen, A.T., Hentzer, M., Sternberg, C., Givskov, M., Ersbøll, B.K. and
643 Molin, S. (2000) Quantification of biofilm structures by the novel computer program
644 COMSTAT. *Microbiology* 146(10), 2395-2407.
- 645 Hijnen, W.A.M., Biraud, D., Cornelissen, E.R. and van der Kooij, D. (2009) Threshold
646 Concentration of Easily Assimilable Organic Carbon in Feedwater for Biofouling of Spiral-
647 Wound Membranes. *Environmental Science & Technology* 43(13), 4890-4895.
- 648 Hong, S. and Elimelech, M. (1997) Chemical and physical aspects of natural organic matter
649 (NOM) fouling of nanofiltration membranes. *Journal of Membrane Science* 132(2), 159-181.
- 650 Hwang, G., Kang, S., El-Din, M.G. and Liu, Y. (2012) Impact of conditioning films on the
651 initial adhesion of *Burkholderia cepacia*. *Colloids and Surfaces B: Biointerfaces* 91(0), 181-
652 188.
- 653 Hwang, G., Liang, J., Kang, S., Tong, M. and Liu, Y. (2013) The role of conditioning film
654 formation in *Pseudomonas aeruginosa* PAO1 adhesion to inert surfaces in aquatic
655 environments. *Biochemical Engineering Journal* 76(0), 90-98.
- 656 King, E.O., Ward, M.K. and Raney, D.E. (1954) Two Simple Media for the Demonstration of
657 Pyocyanin and Fluorescin. *Journal of Laboratory and Clinical Medicine* 44(2), 301-307.
- 658 Lagendijk, E.L., Validov, S., Lamers, G.E.M., de Weert, S. and Bloemberg, G.V. (2010)
659 Genetic tools for tagging Gram-negative bacteria with mCherry for visualization in vitro and
660 in natural habitats, biofilm and pathogenicity studies. *Fems Microbiology Letters* 305(1), 81-
661 90.

662 Lee, Y.-H., Chang, J.-J., Lai, W.-F., Yang, M.-C. and Chien, C.-T. (2011) Layered hydrogel
663 of poly (γ -glutamic acid), sodium alginate, and chitosan: Fluorescence observation of
664 structure and cytocompatibility. *Colloids and Surfaces B: Biointerfaces* 86(2), 409-413.

665 Li, B. and Logan, B.E. (2004) Bacterial adhesion to glass and metal-oxide surfaces. *Colloids*
666 *and Surfaces B: Biointerfaces* 36(2), 81-90.

667 Liikanen, R., Yli-Kuivila, J. and Laukkanen, R. (2002) Efficiency of various chemical
668 cleanings for nanofiltration membrane fouled by conventionally-treated surface water.
669 *Journal of Membrane Science* 195(2), 265-276.

670 Listiarini, K., Chun, W., Sun, D.D. and Leckie, J.O. (2009) Fouling mechanism and
671 resistance analyses of systems containing sodium alginate, calcium, alum and their
672 combination in dead-end fouling of nanofiltration membranes. *Journal of Membrane Science*
673 344(1-2), 244-251.

674 Liu, C.X., Zhang, D.R., He, Y., Zhao, X.S. and Bai, R. (2010) Modification of membrane
675 surface for anti-biofouling performance: Effect of anti-adhesion and anti-bacteria approaches.
676 *Journal of Membrane Science* 346(1), 121-130.

677 Lorite, G.S., Rodrigues, C.M., de Souza, A.A., Kranz, C., Mizaikoff, B. and Cotta, M.A.
678 (2011) The role of conditioning film formation and surface chemical changes on *Xylella*
679 *fastidiosa* adhesion and biofilm evolution. *Journal of Colloid and Interface Science* 359(1),
680 289-295.

681 Mueller, L.N., De Brouwer, J.F., Almeida, J.S., Stal, L.J. and Xavier, J.B. (2006) Analysis of
682 a marine phototrophic biofilm by confocal laser scanning microscopy using the new image
683 quantification software PHLIP. *BMC ecology* 6(1), 1.

684 Ramon, G.Z. and Hoek, E.M.V. (2013) Transport through composite membranes, part 2:
685 Impacts of roughness on permeability and fouling. *Journal of Membrane Science* 425-426(0),
686 141-148.

687 Rana, D. and Matsuura, T. (2010) Surface modifications for antifouling membranes.
688 *Chemical Reviews* 110(4), 2448-2471.

689 Schneider, R.P. (1996) Conditioning Film-Induced Modification of Substratum
690 Physicochemistry—Analysis by Contact Angles. *Journal of Colloid and Interface Science*
691 182(1), 204-213.

692 Semiao, A.J.C., Habimana, O., Cao, H., Heffernan, R., Safari, A. and Casey, E. (2013) The
693 importance of laboratory water quality for studying initial bacterial adhesion during NF
694 filtration processes. *Water Research* 47(8), 2909-2920.

695 Smets, B.F., Grasso, D., Engwall, M.A. and Machinist, B.J. (1999) Surface physicochemical
696 properties of *Pseudomonas fluorescens* and impact on adhesion and transport through porous
697 media. *Colloids and Surfaces B: Biointerfaces* 14(1-4), 121-139.

698 Subramani, A. and Hoek, E.M.V. (2008) Direct observation of initial microbial deposition
699 onto reverse osmosis and nanofiltration membranes. *Journal of Membrane Science* 319(1-2),
700 111-125.

701 Subramani, A., Huang, X. and Hoek, E.M.V. (2009) Direct observation of bacterial
702 deposition onto clean and organic-fouled polyamide membranes. *Journal of Colloid and*
703 *Interface Science* 336(1), 13-20.

704 Tang, C.Y., Kwon, Y.-N. and Leckie, J.O. (2007) Characterization of humic acid fouled
705 reverse osmosis and nanofiltration membranes by transmission electron microscopy and
706 streaming potential measurements. *Environmental Science & Technology* 41(3), 942-949.

707 Ventresque, C., Gisclon, V., Bablon, G. and Chagneau, G. (2000) An outstanding feat of
708 modern technology: the Mery-sur-Oise nanofiltration Treatment plant (340,000 m³/d).
709 *Desalination* 131(1-3), 1-16.

710 Vrouwenvelder, J.S., Beyer, F., Dahmani, K., Hasan, N., Galjaard, G., Kruithof, J.C. and Van
711 Loosdrecht, M.C.M. (2010) Phosphate limitation to control biofouling. *Water Research*
712 44(11), 3454-3466.

713 Vrouwenvelder, J.S., Manolarakis, S.A., van der Hoek, J.P., van Paassen, J.A.M., van der
714 Meer, W.G.J., van Agtmaal, J.M.C., Prummel, H.D.M., Kruithof, J.C. and van Loosdrecht,
715 M.C.M. (2008) Quantitative biofouling diagnosis in full scale nanofiltration and reverse
716 osmosis installations. *Water Research* 42(19), 4856-4868.

717 Wilkinson, K.J., Balnois, E., Leppard, G.G. and Buffle, J. (1999) Characteristic features of
718 the major components of freshwater colloidal organic matter revealed by transmission
719 electron and atomic force microscopy. *Colloids and Surfaces A: Physicochemical and*
720 *Engineering Aspects* 155(2-3), 287-310.

721 Xie, M., Nghiem, L.D., Price, W.E. and Elimelech, M. (2013) Impact of humic acid fouling
722 on membrane performance and transport of pharmaceutically active compounds in forward
723 osmosis. *Water Research* 47(13), 4567-4575.

724 Xu, P., Drewes, J.E., Kim, T.-U., Bellona, C. and Amy, G. (2006) Effect of membrane
725 fouling on transport of organic contaminants in NF/RO membrane applications. *Journal of*
726 *Membrane Science* 279(1-2), 165-175.

727 Yuan, Y. and Kilduff, J.E. (2010) Effect of colloids on salt transport in crossflow
728 nanofiltration. *Journal of Membrane Science* 346(2), 240-249.

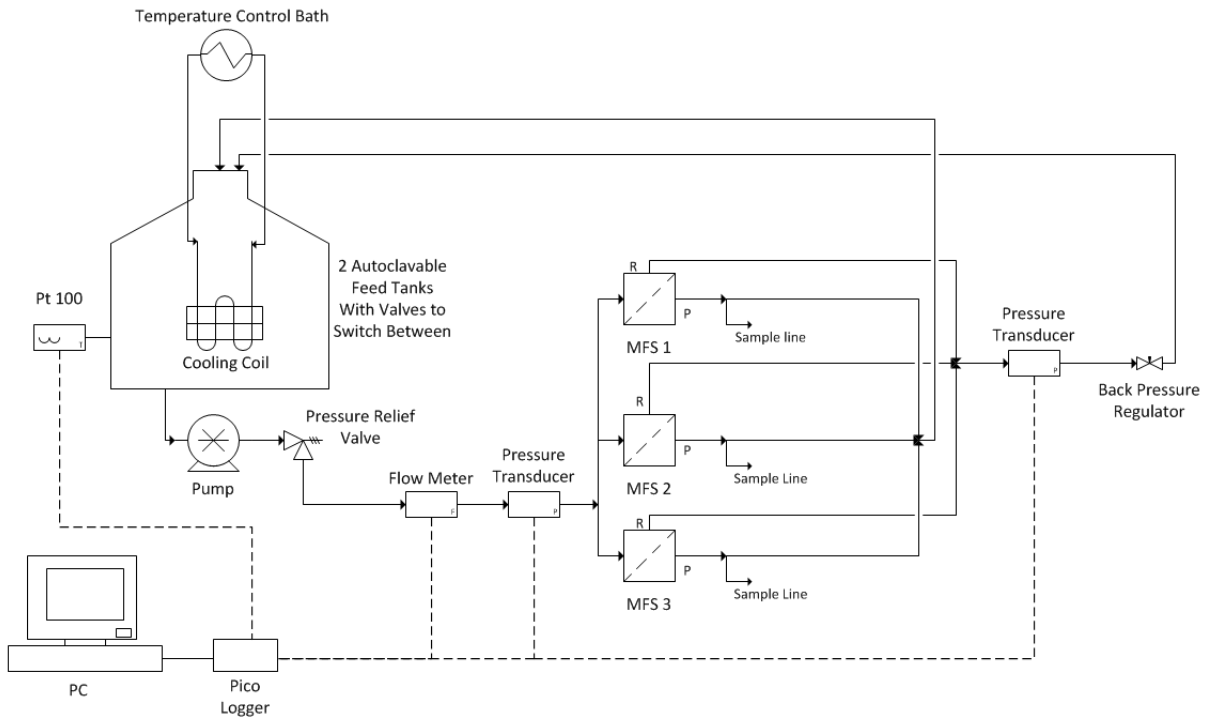
729

730

731

732 **Figures**

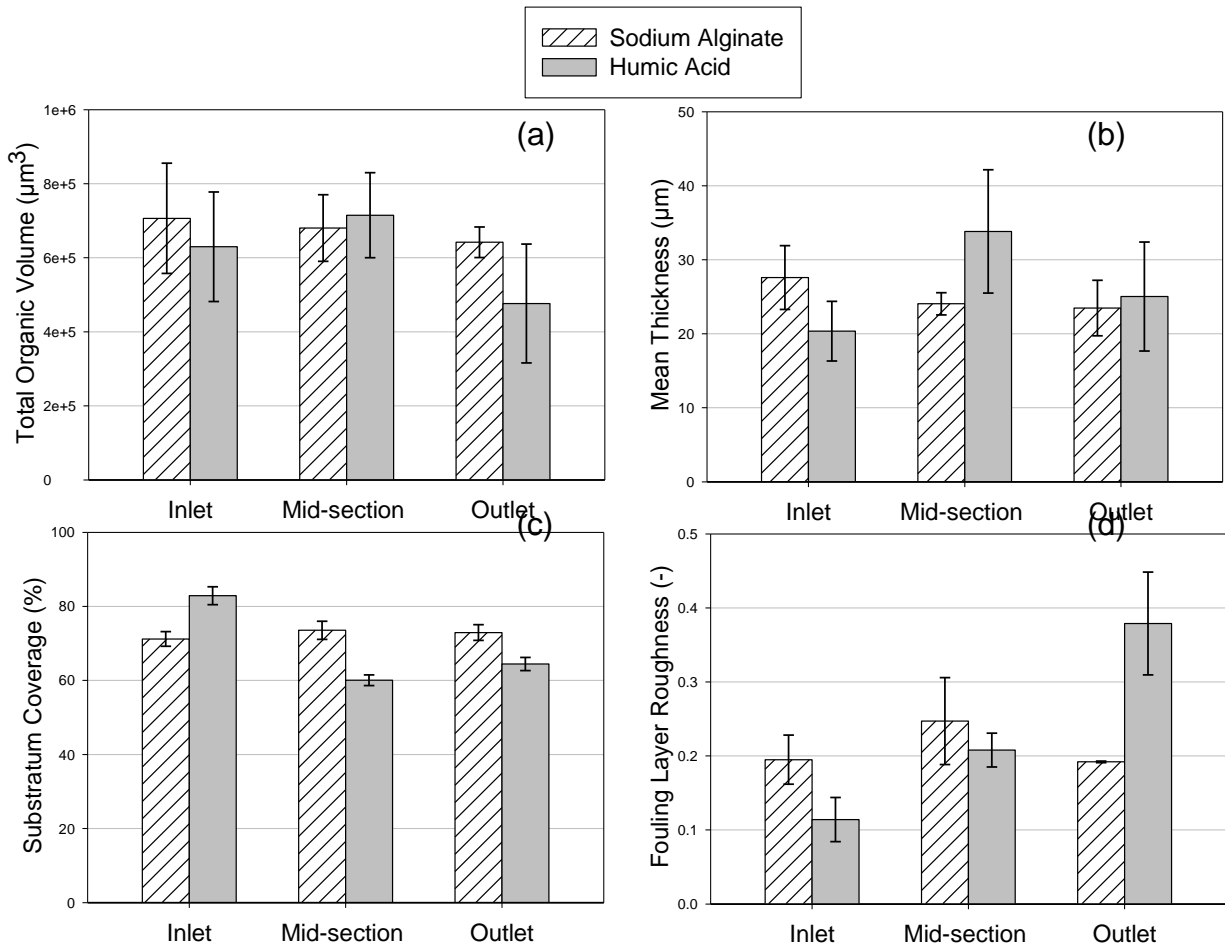
733



734

735 *Figure 1: Crossflow Filtration System Setup*

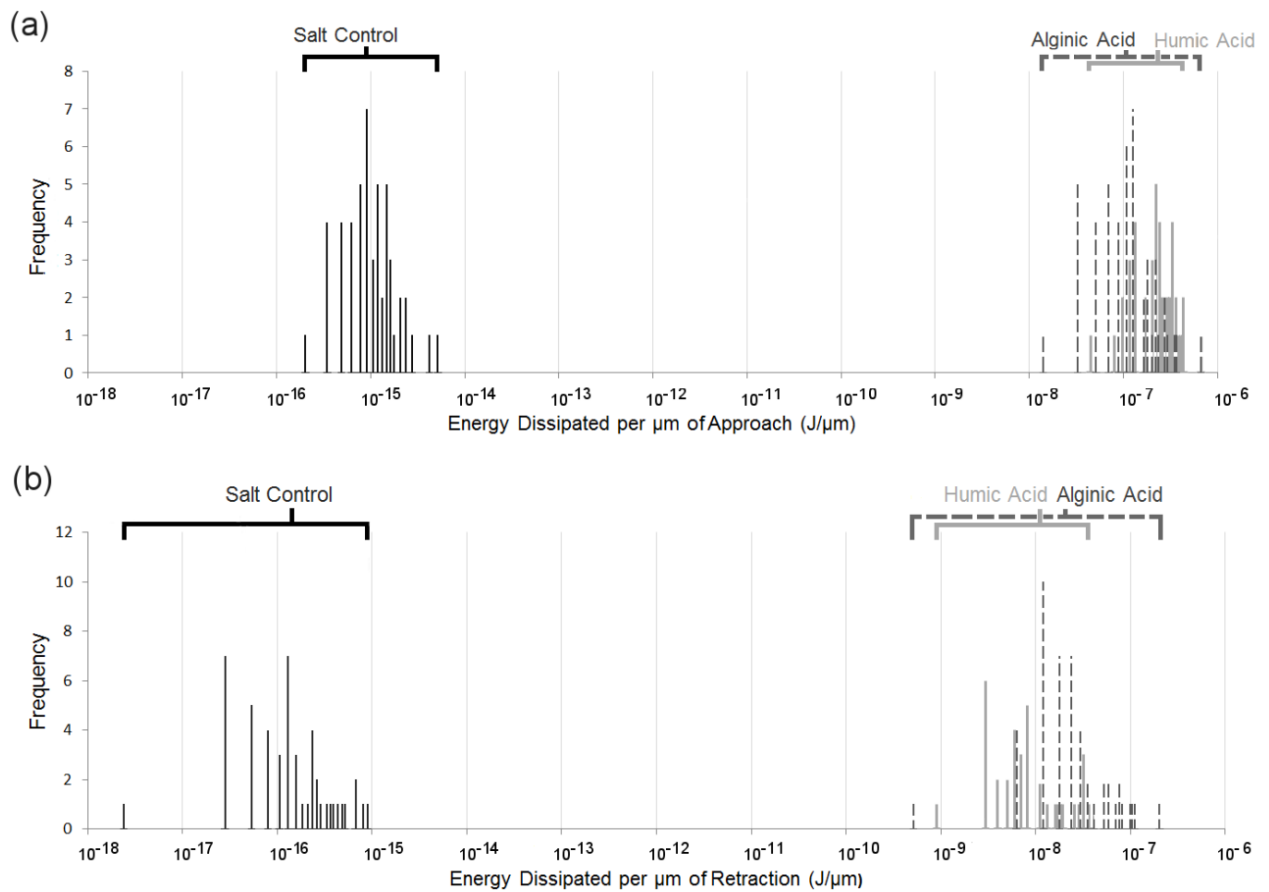
736



737
738

739 *Figure 2: Confocal Microscopy results of NF90 membrane samples fouled with humic acid and alginic acid in*
 740 *cross-flow. Layer properties shown are: (a) total organic volume, (b) layer thickness, (c) surface coverage by*
 741 *the layer, (d) layer roughness. Fouling conditions: 42 LMH permeate flux, 0.39 m/s cross-flow rate. Feed*
 742 *solution: 1 mgC/L humic acid or 2 mgC/L alginic acid, 20 mM NaCl, 1 mM NaHCO₃ and 0.5mM CaCl₂, 20 ± 1*
 743 *°C, pH 8.5.*

744

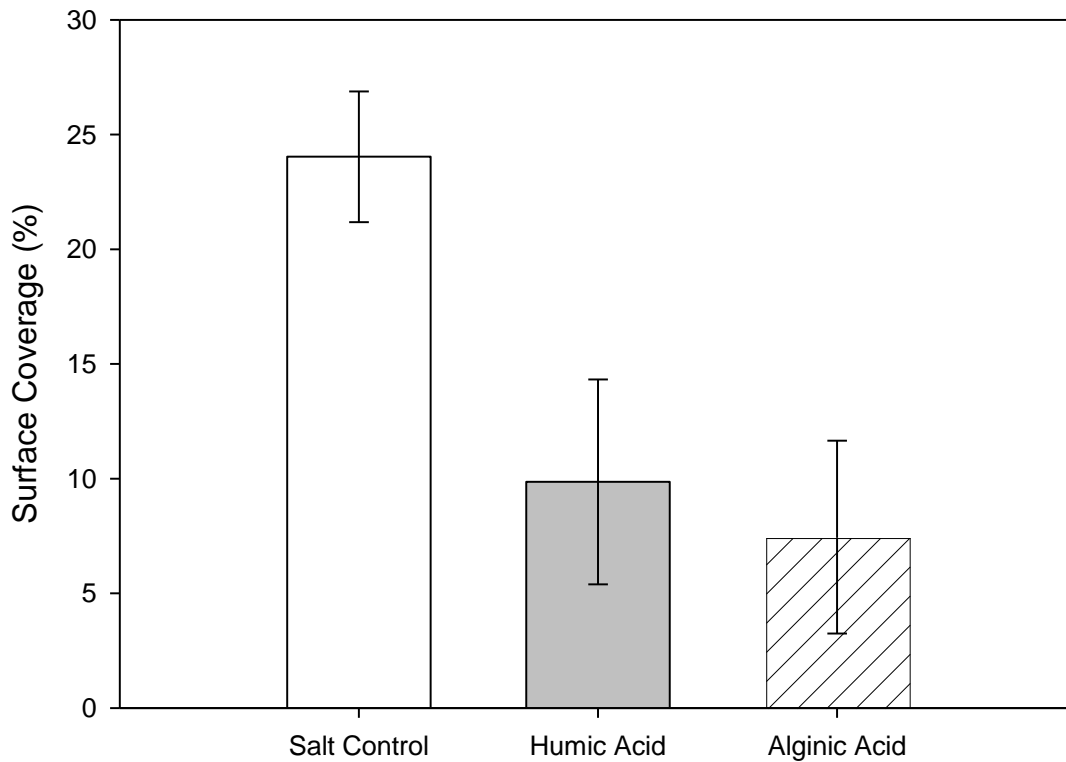


745

746 *Figure 3: Population density diagrams of the energy dissipated during approach (a) and retraction (b) of a*
 747 *triangular silicon nitride Atomic Force Microscopy probe through the top 0.5 - 1 μm of fouling layers of humic*
 748 *acid and alginic acid on NF90 membranes, or within 0.5 μm of an unfouled salt control sample. 50 independent*
 749 *measurements were taken from 8 membrane samples for each foulant and corrected to 1 μm for comparative*
 750 *purposes. Energy dissipated is presented on a \log_{10} scale.*

751

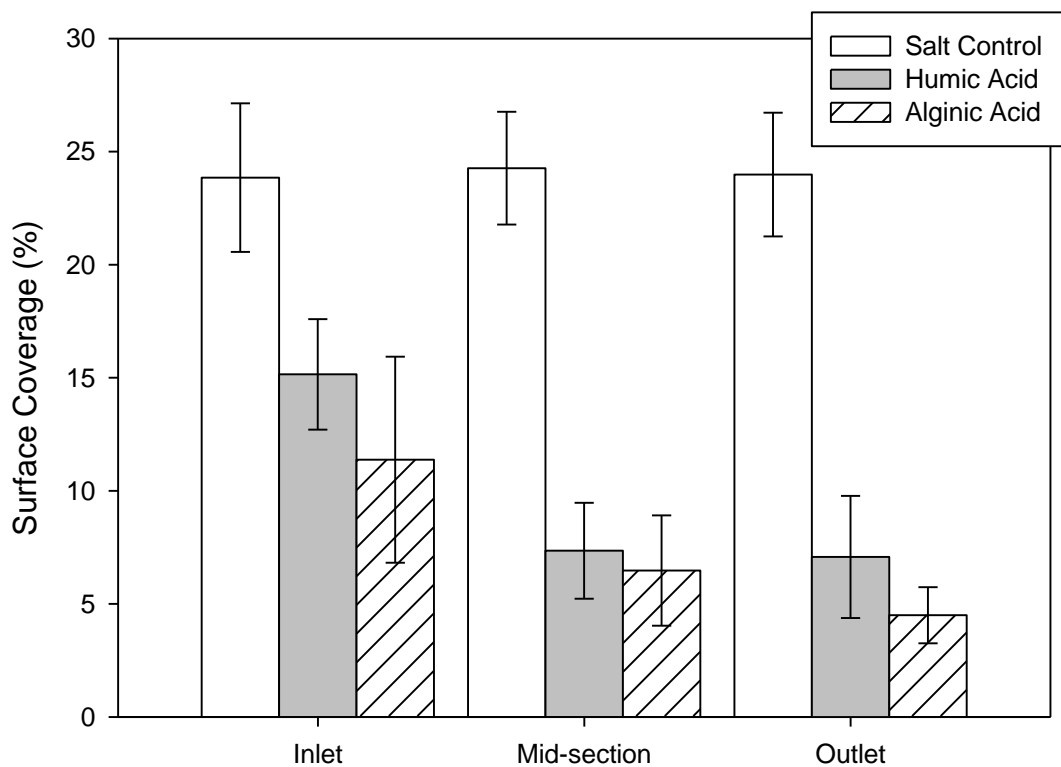
752



753

754 *Figure 4: Surface coverage of Pseudomonas fluorescens cells on NF90 membrane samples fouled with humic*
 755 *acid, alginic acid and a salt control under cross-flow conditions after 30 minutes of initial adhesion (42 LMH*
 756 *permeate flux, 0.39 m/s cross-flow rate). Feed solution: 1mgC/L humic acid or 2mgC/L alginic acid, 20 mM*
 757 *NaCl, 1 mM NaHCO₃ and 0.5 mM CaCl₂, 20 ± 1 °C, pH 8.5. The results shown are the average of at least three*
 758 *samples from all regions of the membrane (inlet, mid-section and outlet) for each feed with the standard*
 759 *deviations shown.*

760



761

762 *Figure 5: Surface coverage of Pseudomonas fluorescens cells on NF90 membrane samples fouled with humic*
 763 *acid, alginic acid and a salt control under cross-flow conditions (42 LMH permeate flux, 0.39 m/s cross-flow*
 764 *rate) after 30 minutes of initial adhesion. Feeds solution: 1mgC/L humic acid or 2mgC/L alginic acid, 20 mM*
 765 *NaCl, 1 mM NaHCO₃ and 0.5 mM CaCl₂, 20 ± 1 °C, pH 8.5. The results shown are the average of at least three*
 766 *samples from each region of the membrane (inlet, mid-section and outlet) for each feed with the standard*
 767 *deviations shown.*

768